This article has been accepted for publication in a future issue of this journal, but has not been fully edited. Content may change prior to final publication. Citation information: DOI 10.1109/TII.2019.2901516, IEEE Transactions on Industrial Informatics

PNKLMF Based Neural Network Control and Learning based HC MPPT Technique for Multi-Objective Grid Integrated Solar PV Based Distributed Generating System

Nishant Kumar, *Member IEEE*, Bhim Singh, *Fellow IEEE* and Bijaya Ketan Panigrahi, *Senior Member IEEE*

***Abstract*—In this work, a novel power normalized kernel least mean fourth algorithm based neural network (NN) control (PNKLMF-NN) technique and learning based hill climbing (L-HC) MPPT (Maximum Power Point Tracking) algorithm, are proposed for grid-integrated solar PV (Photovoltaic) system. Here three-phase single-stage topology of grid-integrated PV system is used, for feeding the nonlinear/linear load at point of common coupling (PCC). A single layer neuron structure is used for active load component (ALC) extraction from distorted load current. During ALC extraction, PNKLMF-NN control very precisely attenuates harmonics components, noise, DC offset, bias, notches and distortions from the nonlinear current, which improves the power quality under normal as well as under abnormal conditions. This single layer PNKLMF-NN control has a very simple architecture, which reduces the computational burden and complexity. Therefore, it is easy in implementation. Moreover, proposed L-HC is the improved form of Hill Climbing (HC) algorithm, where inherent problems of traditional HC algorithm like steady state oscillation, slow dynamic responses and fixed step size issues, are successfully mitigated. The prime objective of proposed PNKLMF-NN control is to meet the active power requirement of the loads from generated solar PV power, and excess power fed into the grid. However, when generated PV power is less than the required load power, then PNKLMF-NN control meets the load by taking extra required power from the grid. During these processes, power quality is maintained at the grid. Moreover, when solar irradiation is zero, VSC (Voltage Source Converter) acts as DSTATCOM (Distribution Static Compensator), which enhances the utilization factor of the system. The proposed techniques are modeled and, their performances are verified experimentally on a developed prototype, in adverse conditions, which test results have satisfied the objectives of the proposed system and the IEEE-519 standard.**

***Index Terms*—Solar PV, Power Quality, Grid Tied System, Power Normalized Kernel Least Mean Fourth, DSTATCOM.**

Nomenclature

L_{VSC}	Interfacing inductors
R_r, C_r	Resistance and capacitor of ripple filter
v_{sab}, v_{sbc}	Grid line voltages
v_{sa}, v_{sb}, v_{sc}	3-phase grid voltages
v_a, v_b, v_c	In-phase quantities of grid voltages
ω	Natural frequency
T_s	Sampling time period
V_x	Amplitude of grid voltage
u_a, u_b, u_c	In-phase unit-templates
P_{PV}	PV power
I_{Dpv}	PV dynamic reflection component
V_{DCref}	DC link reference voltage
V_{DC}	DC link voltage
e_{DC}	DC link voltage error
β_{DC}	DC loss component
G_{I1} , G_{P1}	Integral and proportional gains of PI controller
i_{qa}*, i_{qb}*, i_{qc}*	Reference grid currents
i_{ga}, i_{gb}, i_{gc}	Grid currents
ξ_{pa}, ξ_{pb}, ξ_{pc}	Active weight components
i_{La}, i_{Lb}, i_{Lc}	Load currents
Φ_p	Resultant active weight component
ξ_p	Resultant estimated active weight component
d_{base}	Base step size
rn	Step size
$R1$	Previous DC link reference voltage
ϕ_{pa}	Prediction error
$\xi_{pa}(n)$, $\xi_{pb}(n)$, $\xi_{pc}(n)$	Active weight of load current for phase ‘a’, phase ‘b’ and phase ‘c’
Ω	Learning rate of $\xi_{pa}(n)$
ε	Scaling factor
δ	Normalizing factor
$\sigma_{pa}(n)$	Autocorrelation factor of the active component for phase ‘a’
$\mu_{pa}(n)$	Active weight constant for phase ‘a’
τ and ς	Accelerating parameters
ϑ	Autocorrelation parameter

Manuscript received June 10, 2018; revised November 14, 2018, and accepted Feb. 20, 2019. This work was supported by the Department of Science and Technology, Government of India, Joint UK-India Clean Energy (JUICE) Project, under Grant: RP03391G. and JC Bose fellowship, under Grant: RP03128. (Corresponding author: Nishant Kumar.)

N. Kumar, B. Singh, and B. K. Panigrahi are with the Department of Electrical Engineering, Indian Institute of Technology Delhi, New Delhi 110 016, India (e-mail:, nishant.kumar1729@gmail.com; bhimsinghiitd61@gmail.com; bijayaketan.panigrahi@gmail.com).

I. Introduction

THE generation from distributed resources, such as solar PV (photovoltaic) is very popular. The most popular way of generation is from the rooftop solar PV array. However, the operation in standalone mode is not reliable, because of the variable behaviour of environmental climate. Therefore, the amount of solar PV power is also varied, and it is not always equal to the load. Sometimes, it is higher than the load, so required a power sink, and sometimes, it is lower than the load, so required a power source. In this situation, grid-connected solar PV system is the best option, because according to the situation, the grid can behave as sink and source. Mainly, single stage and two stage systems are the most popular way of solar PV integration with the grid, through a VSC (Voltage Source Converter) [1]. In two-stage topology, one separate DC-DC converter is used for maximum power point tracking

This article has been accepted for publication in a future issue of this journal, but has not been fully edited. Content may change prior to final publication. Citation information: DOI 10.1109/TII.2019.2901516, IEEE Transactions on Industrial Informatics

(MPPT), and one separate DC-AC converter is used for power conversion as well as for grid synchronization [2]. However, in single stage topology, only one DC-AC converter is used for MPPT and power conversion, for both purposes. Therefore, the total converter loss is very less, w.r.t. two stage topology, which enhances the efficiency of the system. Moreover, the required space and circuitry complexity are also less.

However, a robust control for VSC (Voltage Source Converter) is needed for efficient operation, because the responsibilities of that control technique are, 1) maximum power extraction from PV array, 2) power conversion from DC to AC, 3) to follow the grid code for synchronization with the grid, 4) improvement of power quality of the supply power, 5) it acts as DSTATCOM (Distribution Static Compensator), when solar irradiation is zero, and 6) power management, means generated power is used to satisfy the load demand, after fulfiling the load demand, the rest power is supplied to the grid. However, when generated power is not sufficient for the load, then the load requirement is met by taking extra required power from the grid.

Recently, neural network (NN) based control techniques are more popular. Because recent advancement in NN has reduced the computational burden and algorithm complexity, so on wide range NN based control techniques are used in the online system [3]. In order to make control fast and increase the decision taking ability, NN based control techniques are popular in grid integration system. Today, due to generic nature and parallel computation, frequently NN has applied in almost every control technique. Lin *et al.* [4] have given model articulation neural network based power control for active power control and fuzzy neural network control for reactive power control. Cirrincione *et al.* [5] have proposed an adaptive neural filtering for current harmonics compensation. Agarwal *et al.* [6] have proposed least mean square based NN structure for control purpose in the distribution network. Similarly, substantial literature is available, where NN is integrated with conventional control technique.

In-depth literature review on 'control techniques for the grid integrated solar PV system' depicts that in recent time, researchers have proposed several adaptive control algorithms [7], such as fuzzy adaptive control, neuro-fuzzy inference based control [8], delta power control [9], etc. However, for abnormal grid conditions, the performances of these control techniques, are not reported, which is the essential phenomenon of the distribution grid. The other control techniques like, *dq*-transform based SRFT control [10], notch filter based control technique [11] discrete-Fourier transform (DFT), PM (Prony's method), frequency locked loop (FLL), second-order generalized integrator (SOGI) [12], modified SOGI [13][14], LMS (Least Mean Square) [15], LMF (Least Mean Fourth) [16], KF (Kalman Filter) [17], power normalized kernel least mean square [18] etc have been proposed to handle the abnormal grid conditions. However, none of them is suitable for all types of grid adverse conditions, such as FLL and SOGI based control techniques are unable to handle lower order harmonics and DC offset. The fixed length window with stationary waveform, is required for searching in DFT based control technique, which is not suitable for online searching. The performance of PM is appreciable in different grid adverse conditions. However, in the PM technique, the higher order polynomial equation and its solution process, create a huge computational burden on the processor, which is not suitable for the low-cost microcontroller. Similarly, KF based control technique is good for solution estimation using correction and prediction process. Moreover, the modified version of KF, like extended KF [19] and linear KF [20] based control techniques are also good for the integrated grid system. However, during state variable estimation, linearization, prediction and correction, the derivative properties are used, which is the source of burden and algorithm complexity on the processor.

Model predictive control [21] technique is also popular for good steady-state response, but during dynamic condition, it's responses are poor, due to its predictive nature, which is based on the previous dataset. Similarly, resonant controllers, for tracking the sinusoidal inverter current, in grid connected system has been presented in [22], which shows a good steady state response with low harmonics content in injected grid current. However, during transient condition, the performance rapidly deteriorates, due to the changes in the grid frequency.

Therefore, in this work, a novel power normalized kernel least mean fourth based neural network (PNKLMF-NN) control strategy is proposed for optimal control of three-phase single-stage grid-connected solar PV energy conversion system, which is shown in Fig.1. Due to free from derivative operation, the computational complexity and burden are low, in the proposed control technique, Moreover, due to instantaneous performance, this technique is highly suitable for high-frequency system. In this paper, PNKLMF-NN control is described in detail, as well as represented in a block diagram, so it is easy to implement.

Moreover, here, a learning based hill climbing (L-HC) based MPPT (Maximum Power Point Tracking) algorithm is proposed. This L-HC is the improved form of Hill Climbing (HC) algorithm [23], which mitigates the inherent problems of traditional HC algorithm like steady state oscillation, slow dynamic responses and fixed step size issues. A literature review on MPPT shows that many authors have tried to solve these problems through some modifications in classical algorithm namely, modified P&O [24], improved InC (Incremental Conductance) [25], fuzzy logic based MPPT [26], artificial intelligence based MPPT approach, *etc*. However, still, an optimum solution has not come. Because, if few improved techniques are performing well in the steady state then lagging during dynamics, vice versa. Moreover, few techniques are performing relatively well, but the huge computational complexity and large design constraints, restrict to perform on low-cost processor. Therefore, L-HC algorithm is proposed, which simple structure is easy in implementation and its learning nature decides size of step change according to the situation, such as step size decreases during steady state condition, and step size increases during dynamic change.

In this work, the merits of PNKLMF-NN control algorithm and L-HC based MPPT technique, are verified experimentally on a developed prototype, in solar irradiation variation conditions, imbalanced load condition for linear/nonlinear loads, as well as in different grid disturbances such as over-voltage, under-voltage, phase imbalance, harmonics distortion in grid voltage etc. The results show that the obtained voltage current waveforms have satisfied the IEEE-519 and IEEE-1564 standard [27]. In this manuscript, system layout and control approach are described in section-II and section-III, respectively. The results and description are described in section-IV.

This article has been accepted for publication in a future issue of this journal, but has not been fully edited. Content may change prior to final publication. Citation information: DOI 10.1109/TII.2019.2901516, IEEE Transactions on Industrial Informatics

II. System Layout

The system layout of a three-phase single-stage grid-tied solar PV system is shown in Fig.1. The power of PV array is transferred to the grid through a three-phase VSC in one stage, in such a way that the PV array delivers maximum power. The VSC is connected at the PCC (Point of Common Coupling) through L_{VSC} and R_r, C_r, are used to absorb switching ripples generated by VSC [18]. Moreover, the load is also connected on PCC. In this situation, the VSC is controlled in such a way that the PV power is fed into the grid at unity power factor (UPF), and when PV power is zero then it behaves like DSTATCOM.

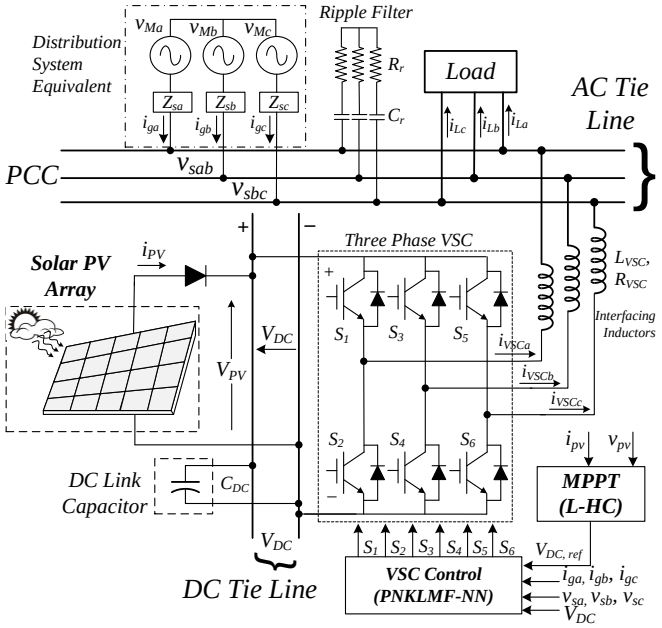

Fig.1 Three-Phase Single-Stage Grid-tied Solar PV System.

III. CONTROL APPROACH

The control strategy for single-stage three-phase grid-tied solar PV array is illustrated in Fig.2. Here, L-HC MPPT algorithm tracks MPP, and PNKLMF-NN control generates reference currents generation. Moreover, from load current, fundamental component is extracted by PNKLMF-NN. Here, first, v_{sab}, and v_{sbc} are sensed at PCC. From them, v_{sa}, v_{sb}, v_{sc} are calculated as,

$$\begin{bmatrix} v_{sa} \\ v_{sb} \\ v_{sc} \end{bmatrix} = \frac{1}{3}\begin{bmatrix} 2 & 1 \\ -1 & 1 \\ -1 & -2 \end{bmatrix}\begin{bmatrix} v_{sab} \\ v_{sbc} \end{bmatrix} \quad (1)$$

A bandpass filter (BPF) is used for filtering the v_{sa}, v_{sb}, v_{sc}, which outputs are v_a, v_b, v_c of grid voltages. The transfer function of the BPF [20] is derived as,

$$T_f = \frac{k(z-1)}{z^2 + (k-2)\times z + \left(1 - k + \frac{k^2}{2}\right)} \quad (2)$$

Where, $k=\sqrt{2}\times\omega\times T_s$.

The V_x is calculated as,

$$V_x = \sqrt{\frac{2}{3}\left(v_a^{\,2} + v_b^{\,2} + v_c^{\,2}\right)} \quad (3)$$

The u_a, u_b, u_c are calculated as,

$$u_a = \frac{v_a}{V_x},\ u_b = \frac{v_b}{V_x},\ u_c = \frac{v_c}{V_x}, \quad (4)$$

For improving the dynamic performances, the instantaneous reflection of change in P_{PV} on i_g is considered by using i_{Dpv} [18]. The I_{Dpv} is defined as,

$$I_{Dpv} = \frac{2\times V_{pv}\times I_{pv}}{3V_x} \quad (5)$$

L-HC algorithm is used for V_{DCref} generation and compared with sensed V_{DC}, which generates e_{DC} (e_{DC} = V_{DCref} - V_{DC}). e_{DC} is send to a PI (Proportional Integral) controller, which produces β_{DC} [18]. β_{DC} is calculated as,

$$\beta_{DC}(n+1) = G_{P1}\times e_{DC}(n) + G_{I1}\times\int_0^t e_{DC}(n)\,dn \quad (6)$$

For generating i_{ga}*, i_{gb}*, i_{gc}*, and to estimate ξ_{pa}, ξ_{pb}, ξ_{pc}, three separate PNKLMF-NN control blocks are used, which are the function of i_{La}, i_{Lb}, i_{Lc}, u_a, u_b, u_c and Φ_p.

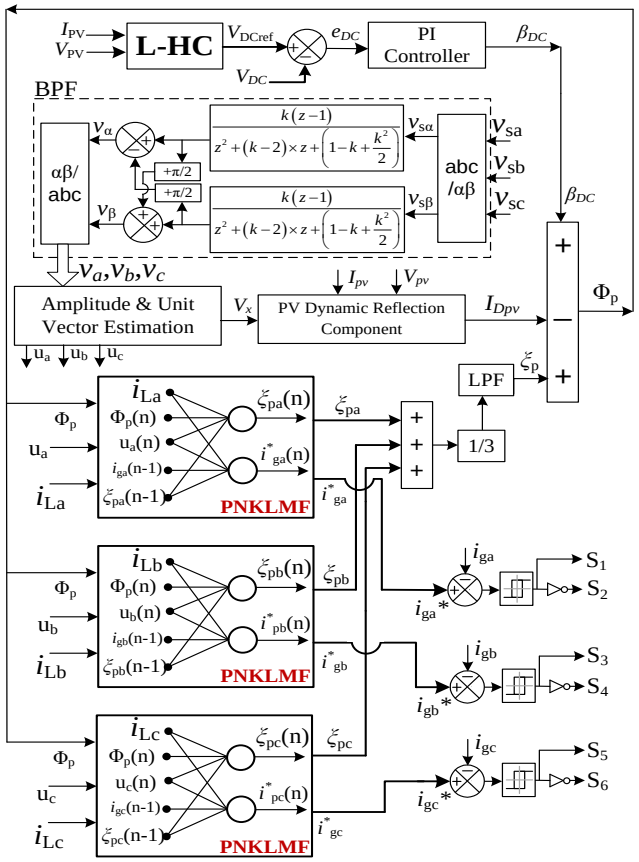

Fig.2 Control scheme for single-stage three-phase grid-tied solar PV system.

$$\left.\begin{aligned} \left[\xi_{Pa}(n),\ \ i^*_{ga}(n)\right] &\Rightarrow f_{\text{PNKLMF}}(i_{La}(n), u_a(n), \Phi_p(n), \xi_{Pa}(n-1), i^*_{ga}(n-1)) \\ \left[\xi_{Pb}(n),\ \ i^*_{gb}(n)\right] &\Rightarrow f_{\text{PNKLMF}}(i_{Lb}(n), u_b(n), \Phi_p(n), \xi_{Pb}(n-1), i^*_{gb}(n-1)) \\ \left[\xi_{Pc}(n),\ \ i^*_{gc}(n)\right] &\Rightarrow f_{\text{PNKLMF}}(i_{Lc}(n), u_c(n), \Phi_p(n), \xi_{Pc}(n-1), i^*_{gc}(n-1)) \end{aligned}\right\} \quad (7)$$

The ξ_p and Φ_p are calculated as,

$$\xi_p = \frac{1}{3}\left(\xi_{pa} + \xi_{pb} + \xi_{pc}\right) \quad (8)$$

$$\Phi_p = \beta_{DC} + \xi_p - I_{Dpv} \quad (9)$$

By using hysteresis controller the switching pulses of VSC (S_1, S_2, S_3, S_4, S_5, and S_6) are produced, where the input signals are i_{ga}, i_{gb}, i_{gc} and i_{ga}*, i_{gb}*, i_{gc}*. The hysteresis controller is a current controller, which controls the VSC.

A. Learning Based Hill Climbing (L-HC) Algorithm

The utilization factor and efficiency of PV array, are improved by using an MPPT algorithm for maximum power extraction. The most popular MPPT techniques are P&O [18], Inc [25] and

This article has been accepted for publication in a future issue of this journal, but has not been fully edited. Content may change prior to final publication. Citation information: DOI 10.1109/TII.2019.2901516, IEEE Transactions on Industrial Informatics

HC. However, the problems with these techniques are, steady state oscillation, slow dynamic responses and fixed step size issues. Therefore, for mitigating the all above problems, a novel L-HC algorithm is proposed here.

Fig.3 and Fig.4 show the working strategy of L-HC technique, which is divided into two parts. 1st section deals with the steady state situation after that mitigates oscillation, by reducing the size of step change. Moreover, 2nd section deals with the dynamic change condition after that quickly jumps on required reference DC link voltage, by increasing the size of step change. For sensing the condition, an envelope is created in each iteration, which upper and lower bands, are *lu* and *ll*, respectively. *lu* and *ll* are calculated according to the d_{base}. *lu* and *ll* are described as,

$$lu = \left(100 + \left(\left(\frac{V_{oc}}{1-d_{base}}\right) - V_{oc}\right) \times \frac{100}{V_{mpp}}\right) \times \frac{1}{100} \tag{10}$$

$$ll = \left(100 - \left(\left(\frac{V_{oc}}{1-d_{base}}\right) - V_{oc}\right) \times \frac{100}{V_{mpp}}\right) \times \frac{1}{100} \tag{11}$$

$$\left.\begin{array}{ll} (lu \times p1) >= p >= (ll \times p1) & \Rightarrow Steady\ State\ Condition \\ else & \Rightarrow Dynamic\ Change\ Condition \end{array}\right\} \tag{12}$$

In dynamic change condition, the change in *rn* is described as,

$$\left|\frac{p-p1}{p1} \times 100\right| \Rightarrow \left.\begin{array}{ll} if <= 10, & \rightarrow rn = r_{base}/2 \\ if else <= 50 \rightarrow & rn = r_{base} \\ else & \rightarrow rn = 2 \times r_{base} \end{array}\right\} \tag{13}$$

In steady state condition, it stores the addition of first 3 conjugative duty cycles in variable '*nl*' and, after this, it stores addition of second 3 conjugative duty cycles in variable '*ml*'. Here *rn* is calculated as,

$$\left.\begin{array}{ll} if \ |ml - nl| == rn1, & \Rightarrow n = 0,\ rn = rn1/2 \\ \text{else} \quad , & \Rightarrow n = ml,\ rn = rn1 \end{array}\right\} \tag{14}$$

After *rn* calculation, it follows the logics for new V_{DCref} calculation, which is described as,

$$\left.\begin{array}{l} if \ \ p > p1 \ \ \&\& \ V > V1 \\ if \ \ p < p1 \ \ \&\& \ V < V1 \end{array}\right\} \Rightarrow \ Z = +1 \Bigg\} R = R1 + Z \times rn \tag{15}$$
$$Else \quad \Rightarrow \ Z = -1 \Big\}$$

Where, *dp=p-p1*, *dV=V-V1*, and *di=i-i1*. The flowchart and block model of L-HC algorithm are given in Fig.3 and Fig.4, respectively.

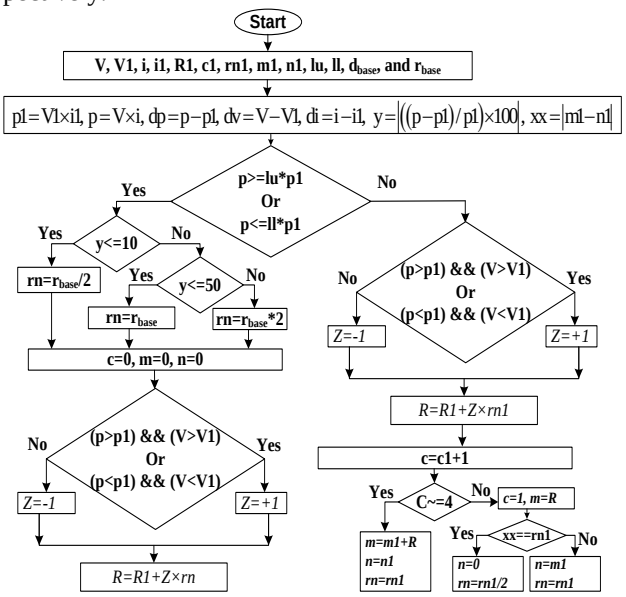

Fig.3 Flowchart of L-HC algorithm.

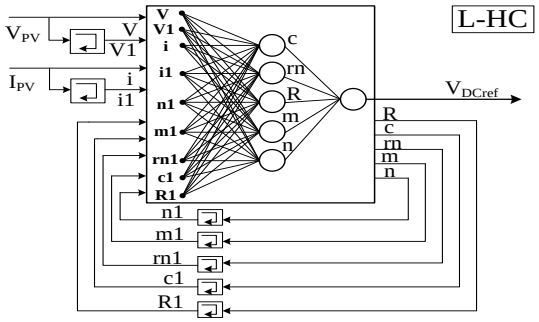

Fig.4 Block model of L-HC algorithm.

Steady-state and dynamic behaviors of L-HC algorithm are shown in Fig.5, which shows the oscillation reduction in steady state condition and sudden jump in dynamic conditions.

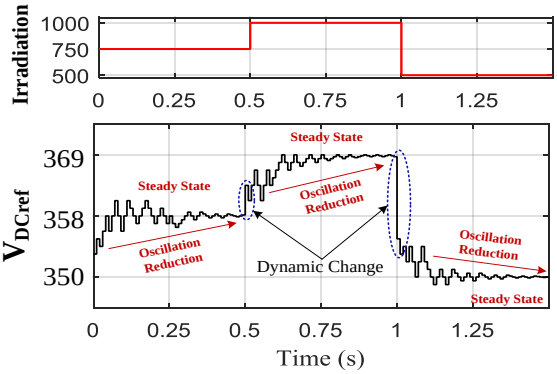

Fig.5 Steady-state and dynamic behavior of L-HC algorithm.

B. Power Normalized Kernel Least Mean Fourth Algorithm

The PNKLMF-NN algorithm is the hybridization of normalized power kernel trick [28] and LMF algorithm. Here, for improving the accuracy, with the help of power kernel trick, mapping in High-Dimensional Space (HDS) technique is used. Normalized power kernel trick realizes the linear relationship in between the input signal during mapping into the HDS. For internal error minimization, least mean fourth algorithm is used. The other advantage PNKLMLF-NN algorithm is, without prior information of the coordinates, the input signals can smoothly map into the HDS. Schematic of adaptive filter based system identification and weight estimation structure of PNKLMF-NN algorithm are shown in Fig.6. Moreover, the block diagram of PNKLMF-NN algorithm for phase 'a' is shown in Fig.7.

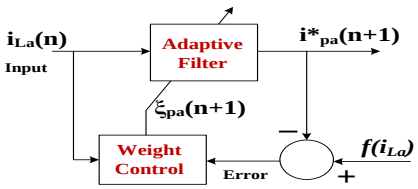

Fig.6 System identification model based on GDLSR.

Here by using PNKLMF-NN, the ϕ_{pa} of active component of load current for phase 'a' is calculated as,

$$\phi_{pa}(n) = i_{La}(n) - u_a(n) \times \xi_{pa}(n) \tag{16}$$

Through optimal updating of $\xi_{pa}(n)$, the ϕ_{pa} is minimized, which is described as,

$$\xi_{pa}(n+1) = \left(1 - \Omega \times \mu_{pa}(n)\right) \times \xi_{pa}(n) + \frac{2\mu_{pa}(n)}{\left\langle \mu_{pa}(n), \sigma_{pa}(n) \right\rangle} \times u_a(n) \times \left(\phi_{pa}(n)\right)^3 \tag{17}$$

This article has been accepted for publication in a future issue of this journal, but has not been fully edited. Content may change prior to final publication. Citation information: DOI 10.1109/TII.2019.2901516, IEEE Transactions on Industrial Informatics

Where, $<\mu_{pa}(n), \sigma_{pa}(n)>$ is function of power kernel trick, for phase 'a', which is calculated as,

$$\left\langle \mu_{pa}(n), \sigma_{pa}(n) \right\rangle = K_{fa}\left(\mu_{pa}(n), \sigma_{pa}(n)\right) = 1 - \frac{\left\| \mu_{pa}(n) - \sigma_{pa}(n) \right\|}{\varepsilon} \quad (18)$$

Through scaling factor, the normalized function of power kernel trick, for phase 'a' is derived as,

$$K_{fna}\left(\mu_{pa}(n), \sigma_{pa}(n)\right) = 1 - \delta \times \frac{\left\| \mu_{pa}(n) - \sigma_{pa}(n) \right\|}{\varepsilon} \quad (19)$$

$\sigma_{pa}(n)$ and $\mu_{pa}(n)$ are calculated as,

$$\sigma_{pa}(n+1) = \vartheta \times \sigma_{pa}(n) + (1-\vartheta) \times \phi_{pa}(n) \times \phi_{pa}(n-1) \quad (20)$$

$$\mu_{pa}(n+1) = \tau \times \mu_{pa}(n) + \varsigma \times \left(\sigma_{pa}(\mathrm{n}+1)\right)^2 \quad (21)$$

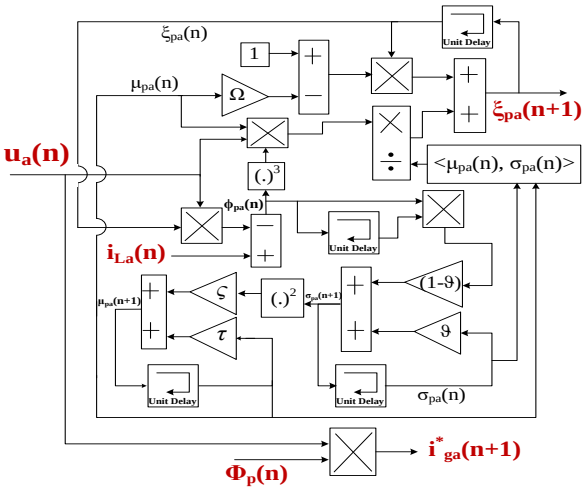

Fig.7 Block diagram of PNKLMF-NN.

In similar way, $\xi_{pb}(n)$, and $\xi_{pc}(n)$ are generated as,

$$\left.\begin{aligned} \phi_{pb}(\mathrm{n}) &= i_{Lb}(\mathrm{n}) - \mathrm{u}_b(n) \times \xi_{pb}(n) \\ \xi_{pb}(n+1) &= \left(1 - \Omega \times \mu_{pb}(n)\right) \times \xi_{pb}(n) + \frac{2\mu_{pb}(n)}{\left\langle \mu_{pb}(n), \sigma_{pb}(n) \right\rangle} \times \mathrm{u}_b(n) \times \left(\phi_{pb}(n)\right)^3 \\ \left\langle \mu_{pb}(n), \sigma_{pb}(n) \right\rangle &= 1 - \delta \times \frac{\left\| \mu_{pb}(n) - \sigma_{pb}(n) \right\|}{\varepsilon} \\ \sigma_{pb}(n+1) &= \vartheta \times \sigma_{pb}(n) + (1-\vartheta) \times \phi_{pb}(n) \times \phi_{pb}(n-1) \\ \mu_{pb}(n+1) &= \tau \times \mu_{pb}(n) + \varsigma \times \left(\sigma_{pb}(\mathrm{n}+1)\right)^2 \end{aligned}\right\} \quad (22)$$

$$\left.\begin{aligned} \phi_{pc}(\mathrm{n}) &= i_{Lc}(\mathrm{n}) - \mathrm{u}_c(n) \times \xi_{pc}(n) \\ \xi_{pc}(n+1) &= \left(1 - \Omega \times \mu_{pc}(n)\right) \times \xi_{pc}(n) + \frac{2\mu_{pc}(n)}{\left\langle \mu_{pc}(n), \sigma_{pc}(n) \right\rangle} \times \mathrm{u}_c(n) \times \left(\phi_{pc}(n)\right)^3 \\ \left\langle \mu_{pc}(n), \sigma_{pc}(n) \right\rangle &= 1 - \delta \times \frac{\left\| \mu_{pc}(n) - \sigma_{pc}(n) \right\|}{\varepsilon} \\ \sigma_{pc}(n+1) &= \vartheta \times \sigma_{pc}(n) + (1-\vartheta) \times \phi_{pc}(n) \times \phi_{pc}(n-1) \\ \mu_{pc}(n+1) &= \tau \times \mu_{pc}(n) + \varsigma \times \left(\sigma_{pc}(\mathrm{n}+1)\right)^2 \end{aligned}\right\} \quad (23)$$

The PNKLMF-NN based control structure for three-phase load component extraction is shown in Fig.8.

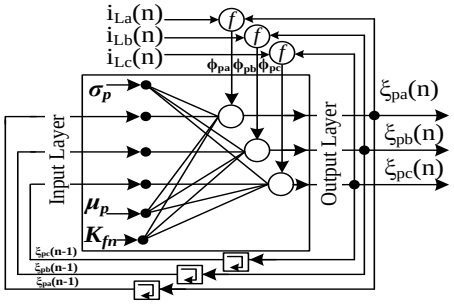

Fig.8 Control structure of weight updating process.

The i_{ga}^*, i_{gb}^*, i_{gc}^* are calculated as,

$$i_{ga}^* = \Phi_p \times u_a, \quad i_{gb}^* = \Phi_p \times u_b, \quad i_{gc}^* = \Phi_p \times u_c \quad (24)$$

C. Comparative Analysis of Proposed PNKLMF-NN Algorithm

The comparative analysis of proposed PNKLMF-NN control algorithm with most popular adaptive algorithms, such as LMS [15], LMF [16], LLMF and normalized LMS (NLMS) is shown in Fig.9.

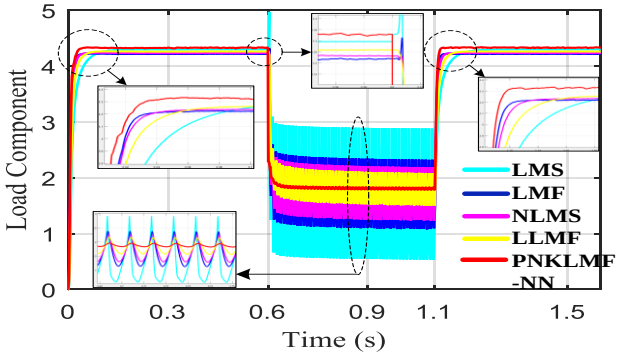

Fig.9 Responses of different algorithms.

For comparative analysis, the unbalanced load situation is considered, where the outage of one phase load for the period of 0.6s to 1.1s, is considered. Fig.9 shows a comparison in the response of fundamental load component extraction from the load current, which is Φ_p. In term of oscillations, Fig.9 shows that during load unbalance, the highest oscillations are in LMS and lowest in PNKLMF-NN. Similarly, in terms of settling time and accuracy, Fig.9 depicts that higher settling time and lower accuracy are in LMF, while lower settling time and higher accuracy are in PNKLMF-NN, which shows a very good fundamental load component extraction ability of PNKLMF-NN algorithm. The achieved rise time and settling time for PNKLMF-NN are 0.21ms and 1.1ms, respectively.

IV. Results and Discussion

A prototype is developed for performance evaluation of proposed L-HC MPPT algorithm and GDLFR control technique, as shown in Fig.10. To realize the PV characteristic, a solar PV simulator (AMETEK, ETS600x17DPVF) is used [29]-[38], and it is integrated with the actual grid. During integration, for DC PV power to conversion in AC form, MPPT operation, load feeding, and for synchronization a three-phase voltage source converter (VSC) is used. The RC filter and interfacing inductors are used for harmonics and switching ripples mitigation. A dSpace (Digital Signal Processor for Applied and Control Engineering) controller (1202-DSPACE) is used for execution of control techniques. The used system parameters are given in Table I.

TABLE I
SYSTEM PARAMETERS

Parameter	Value	Parameter	Value	Parameter	Value
V_{oc}	200V	v_{sa}	100V	C_{fl}	10μF
I_{sc}	15A	f	50Hz	R_{fl}	10Ω
P_{load}	522W	L_{in}	5mH	ϑ	0.2
τ	0.001	ς	10^{-5}	Ω	0.002
r_{base}	2V	d_{base}	0.01	α	1

This article has been accepted for publication in a future issue of this journal, but has not been fully edited. Content may change prior to final publication. Citation information: DOI 10.1109/TII.2019.2901516, IEEE Transactions on Industrial Informatics

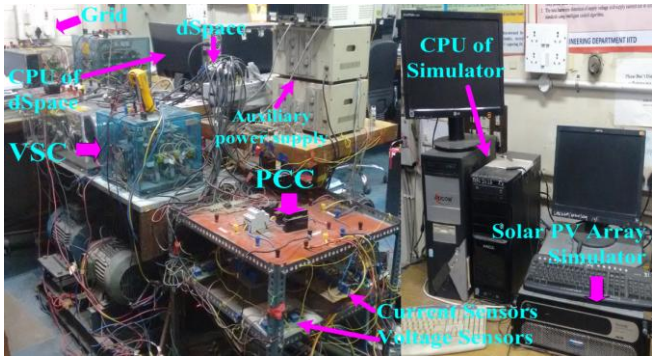

Fig.10 Photograph of the developed prototype.

A. Operation under Normal Condition

For phase 'a', the steady-state responses of the system at nonlinear loads, are shown in Fig.11.

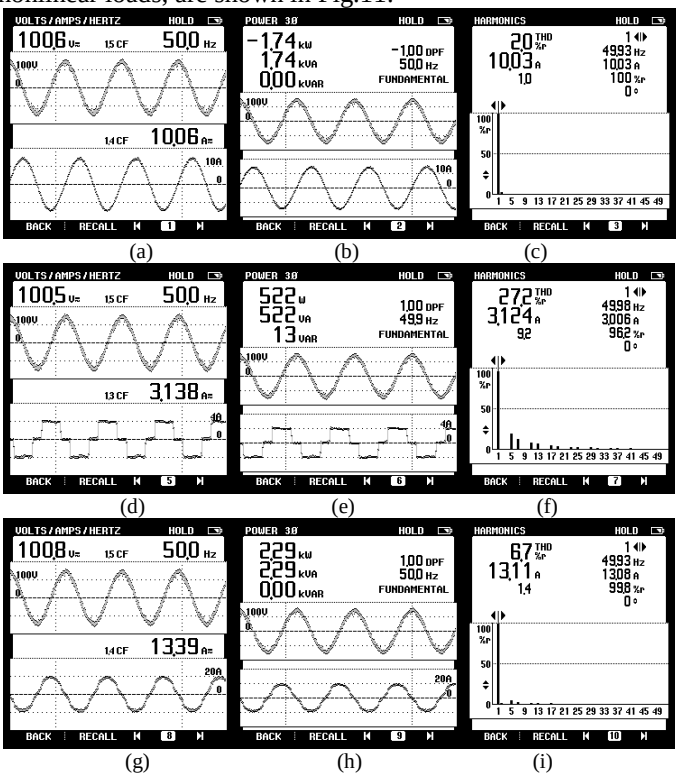

Fig.11 Waveforms of steady-state response for phase 'a', (a)-(c) voltage, current and THD of grid current, (d)-(f) voltage, current and THD of load current, and (g)-(i) voltage, current and THD of VSC current.

Figs.11(d)-(f) show that successfully power is supplied to nonlinear loads, which THD is 27.2%. Moreover, Figs.11(a)-(c) show that after satisfying load demand, rest 1.74kW power is supplied to the grid, where THD of the grid current is 2.0%. It is found good, and within permissible limit of 5% according to the IEEE-519 standard. Figs.11(g)-(i) show the waveforms of VSC power flow, which is supplied by solar PV array and consumed by the load as well as grid. The THD of VSC current is 6.7%. It shows that VSC supplies required harmonics at PCC to the nonlinear load. Therefore, the grid currents are found sinusoidal having THD within the limit.

B. Operation under Load Unbalanced Condition

During unbalanced load condition, load of phase 'a' is removed, and its dynamic effects on phase 'a' and phase 'b' are illustrated in Fig.12(a) and Fig.12(b), respectively, as well as internal signals are shown in Fig.12(c). Fig.12(a) shows that load of phase 'a' removed, so the load current becomes zero. However, due to proper control action, the grid currents are balanced and sinusoidal, as well as DC link voltage is constant. Since, due to outage of phase 'a' load, the requirement of reactive power is reduced, so the shape of VSC current is improved and becomes sinusoidal, as well as nonlinearity of the phase 'b' load current is also reduced, which is shown in Fig.12(b). The performance of internal signals during dynamic condition is shown in Fig.12(c), which shows that DC loss component (β_{DC}) is very less, due to balanced DC link voltage. Moreover, PV dynamic reflection component (I_{Dpv}) is constant, because solar irradiation is assumed constant, and estimated active weight component (ξ_p) is reduced as the requirement of active power is reduced. Therefore, the resultant of all components (Φ_p) is also reduced.

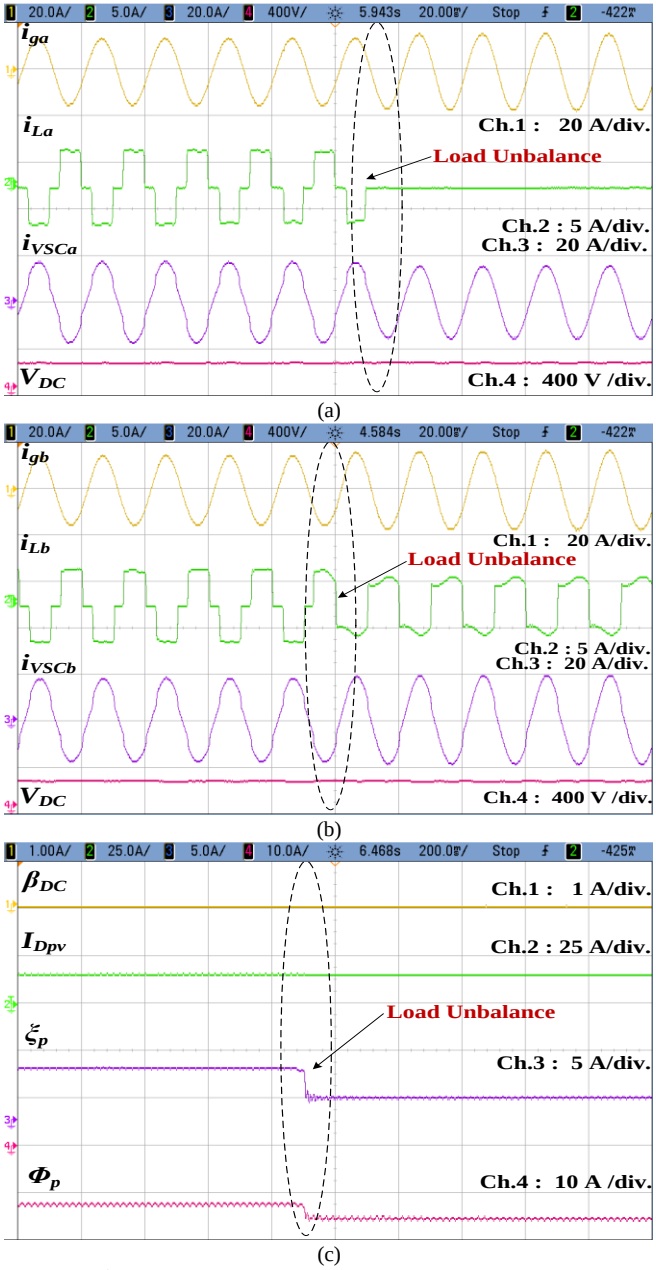

Fig.12 Waveforms during load unbalance, (a)-(b) grid current, load current, VSC current and DC link voltage of phase 'a' and 'b', (c) internel signals.

This article has been accepted for publication in a future issue of this journal, but has not been fully edited. Content may change prior to final publication. Citation information: DOI 10.1109/TII.2019.2901516, IEEE Transactions on Industrial Informatics

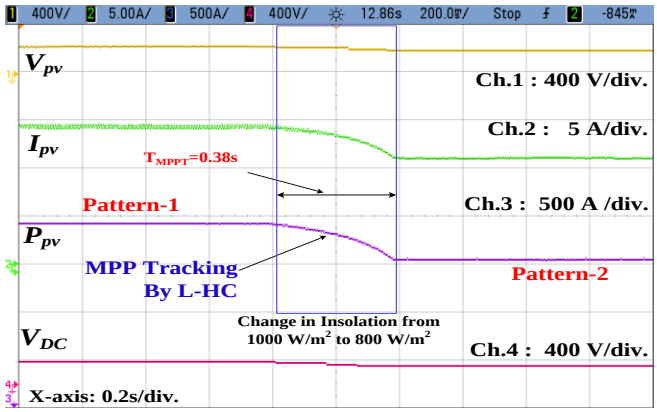

Fig.13 Waveforms during insolation fall.

C. Operation at Solar Irradiation Variation Condition

During solar insolation change condition, it is tested for insolation fall (from 1000W/m^2 to 800W/m^2), as well as tested for insolation rise (from 800W/m^2 to 1000W/m^2), which steady-state performances are shown in Fig.13 and Fig.14.

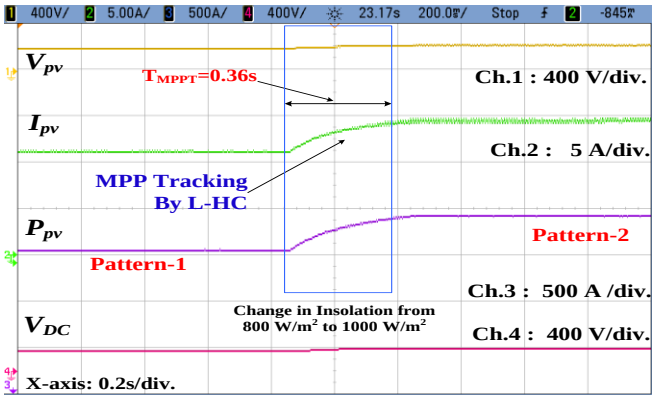

Fig.14 Waveforms during insolation rise.

Fig.13 and Fig.14 show a very smooth and quick maximum power point tracking performance, which is possible only due to proposed L-HC algorithm. Moreover, the steady-state performances in insolation rise and fall condition, at irradiation 1000W/m^2 and 800W/m^2 are oscillation free, which is only due to learning based duty cycle reduction process of L-HC algorithm. After irradiation change, it has taken approximately 0.37s to track the MPP, which shows the excellent dynamic performance of proposed MPPT technique. In both conditions, the tracking efficiency is approximately close to 100%, which shows the accuracy of the L-HC algorithm.

D. Operation during Grid Voltage Fluctuations Condition

During testing for grid voltages fluctuation, over voltage and under voltage conditions are considered. In both conditions, the fluctuation in grid voltage of approximately 15% is taken, which test responses of phase 'a' are shown in Fig.15 and Fig.16. Moreover, harmonic spectra of grid current of phase 'a' for different conditions are shown in Fig.17.

The waveforms shown in Fig.15 depict that due to over-voltage, the v_{sa} at PCC is increased, so due to constant supply power, the i_{ga} is decreased. Moreover, since P_L (load power) is directly propositional to the square of v_{sa}, so P_L, as well as i_{La}, is increased. Similarly, for grid under-voltage condition the performances are illustrated in Fig.16. In both condition, due to strong control ability, the DC link voltage is maintained constant, and a balanced power is supplied to the load. Moreover, after satisfying the load demand, rest solar power is supplied to the grid. During this process, the THD of grid current is still low and within permissible limit of 5% according to the IEEE-519 standard, which is shown in Fig.17.

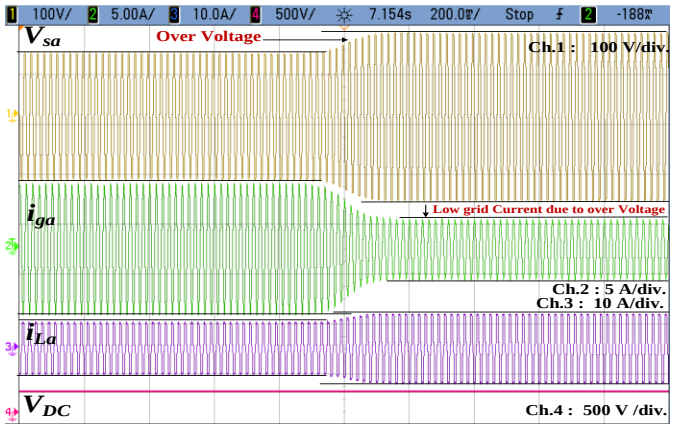

Fig.15 Waveforms during over-voltage condition.

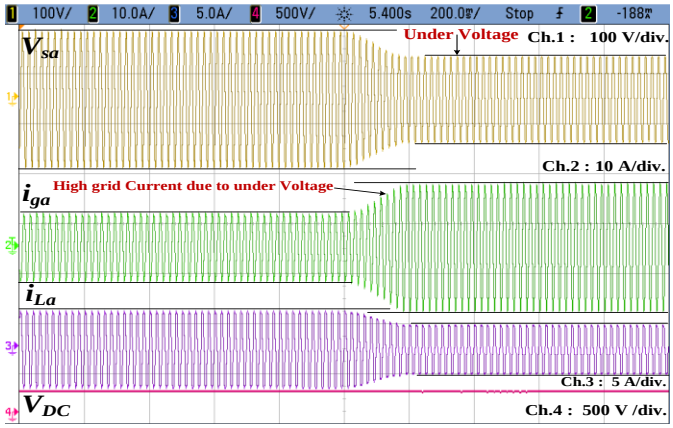

Fig.16 Waveforms during under-voltage condition.

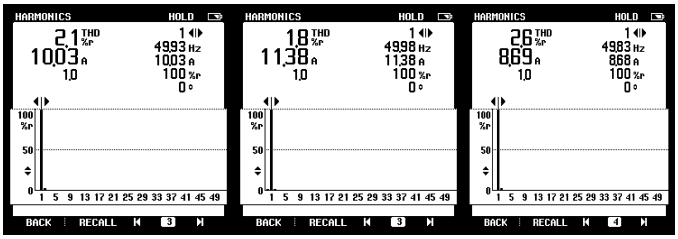

(a) Normal condition (b) Over voltage (c) Under voltage

Fig.17 Waveforms of harmonic spectrum of grid current for phase 'a'.

E. Operation during Grid Voltage Imbalance Condition

The dynamic behavior of the system under imbalance grid voltage condition at solar insolation 500W/m^2, is shown in Fig.18 and, its vector diagram is shown in Fig.19.

From Figs.18-19, it is clearly visible that the three phase voltages are 74.83V, 132.37V and 87.61V, which is a highly imbalance condition. However, in this situation, the three phase currents are 4.902A, 4.905A, and 4.902A, which shows a balanced supply currents. Moreover, the THDs of all three phase grid currents are below 5%, which shows a satisfactory performance.

This article has been accepted for publication in a future issue of this journal, but has not been fully edited. Content may change prior to final publication. Citation information: DOI 10.1109/TII.2019.2901516, IEEE Transactions on Industrial Informatics

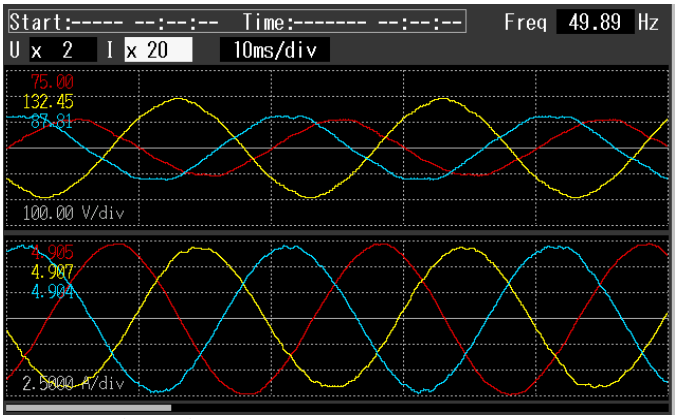

Fig.18 Waveforms of three-phase voltage and current during phase imbalance.

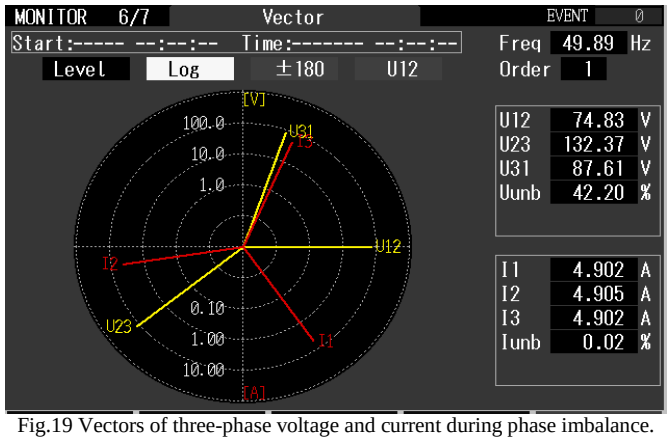

Fig.19 Vectors of three-phase voltage and current during phase imbalance.

F. Operation during Distorted Grid Voltage Condition

The performances in distorted grid voltage condition are shown in Fig.20, and analyzed by using a power analyzer, which obtained waveforms are shown in Fig.21.

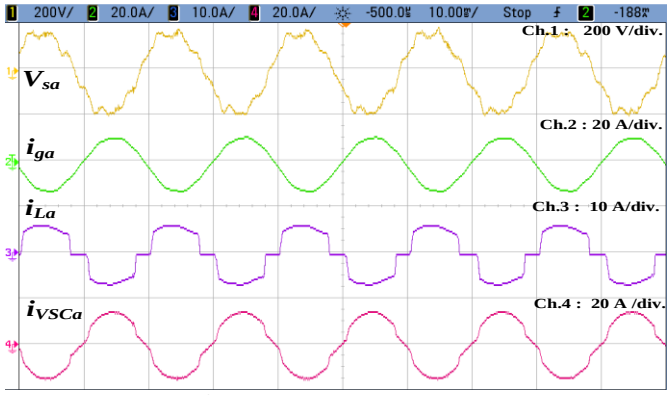

Fig.20 Waveforms under distorted grid voltage condition.

The waveforms for phase ‘a’ are shown in Fig.20 and Fig.21, where the THD of distorted grid voltage is 9.5%, and THD of the nonlinear load current is 36.8%, which are shown in Fig.21(c) and Fig.21(g), respectively. Moreover, for testing of the proposed control technique in a highly complex situation, the overvoltage condition is applied, with distorted grid voltage condition. In this highly nonlinear situation, the proposed control technique has performed very well and properly fed the load. After feeding the load, the rest power is successfully transferred to the grid, where THD of grid current is only 2.4%, at unity power factor, as shown in Fig.21(d).

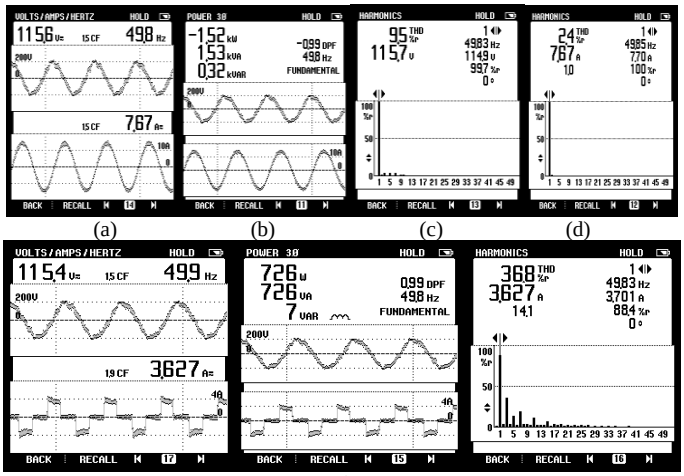

(a) (b) (c) (d)

(e) (f) (g)

Fig.21 Waveforms of, (a)-(d) phase ‘a’ grid voltage, current, power and its harmonic spectrum, and (e)-(f) phase ‘a’ load voltage, current, power and its harmonic spectrum, during distorted grid voltage condition.

G. Operation during Day-to-Night Mode

In day-to-night condition, during the daytime, first solar PV power is used to fulfill the load demand, and if some power is left, then it is fed into the grid. Moreover, during the night time, when solar PV power is zero, then this system behaves like DSTATCOM, where load demand is fed by the grid. The reactive power support to the grid is provided by DSTATCOM. These all performances for day-to-night mode, are shown in Figs.22(a)-(b) and for night-to-day mode are shown in Fig.23(a)-(b).

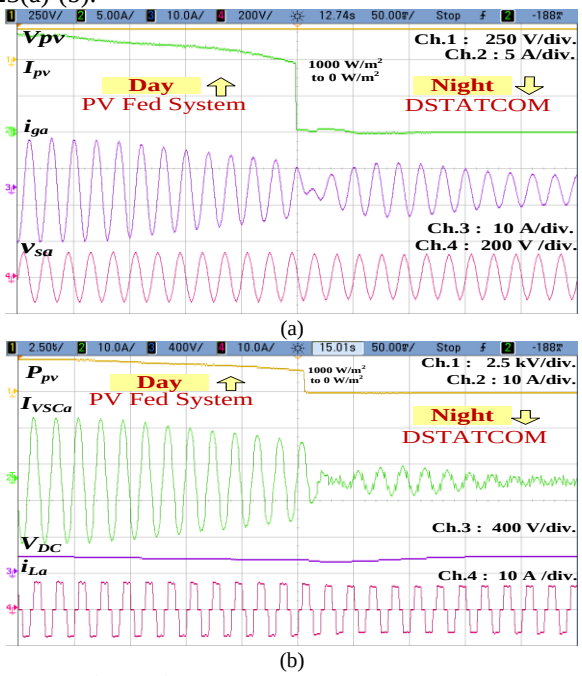

(a)

(b)

Fig.22 Waveforms of day-to-night mode, (a) PV voltage-current and grid voltage-current of phase ‘a’, (b) PV power, VSC current, V_{DC}, and load current of phase ‘a’ for day-to-night and night-to-day condition, respectively.

In Fig.22(a) & Fig.23(a), during the daytime, i_{ga} and v_{sa} are out of phase, which shows that the power is fed into the grid. Moreover, during night time, i_{ga} and v_{sa} are in the same phase, which shows that power is supplied from the grid. The reactive power compensation behavior of the VSC at night time, is shown in Fig.22(b) & Fig.23(b), where it behaves like

This article has been accepted for publication in a future issue of this journal, but has not been fully edited. Content may change prior to final publication. Citation information: DOI 10.1109/TII.2019.2901516, IEEE Transactions on Industrial Informatics

DSTATCOM. It increases the utility of the system. Moreover, in both conditions, the DC link voltage is maintained. Since, it is a single stage topology, so during daytime DC link reference voltage is generated by L-HC MPPT algorithm. However, when PV array current is zero, or PV power is zero, then L-HC algorithm supplies a constant DC link reference voltage (R_{in}), which is used during DSTATCOM operation.

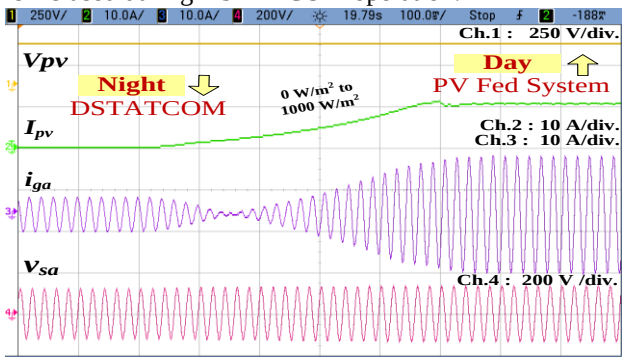

(a)

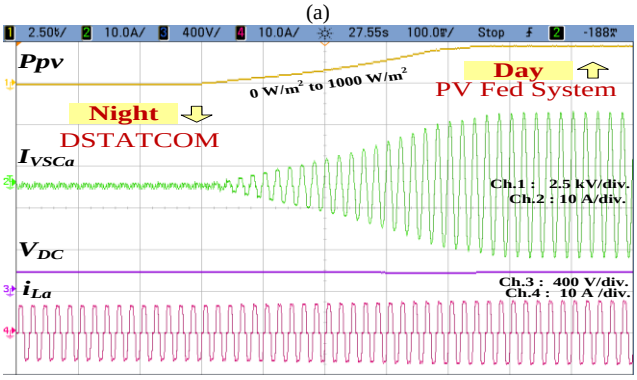

(b)

Fig.23 Waveforms of night-to-day mode, (a) PV voltage-current and grid voltage-current of phase 'a', (b) PV power, VSC current, V_{DC}, and load current of phase 'a' for day-to-night and night-to-day condition, respectively.

V. Conclusion

A novel control technique namely power normalized kernel least mean fourth (PNKLMF-NN) based control algorithm and learning based hill climbing (L-HC) MPPT algorithm, for grid-tied solar PV system have been developed and implemented on the developed prototype, where the nonlinear/linear loads have connected at PCC. The MPPT by L-HC has been shown very good steady state as well as dynamic performance on different types of irradiation conditions. The PNKLMF-NN has enhanced the power management ability with improved power quality, for a single-stage three-phase grid integrated solar PV system, where distribution network subjected to nonlinear loading at, over-voltage, under-voltage, phase imbalance and the distorted voltages at PCC. The simple architecture of the PNKLMF-NN makes easy to implement and helps in computational complexity reduction as well as quick dynamic performance. The performance of PNKLMF-NN has also evaluated on day to night mode of operation. During daytime, the system behaves as PV tied grid system, where the control technique provides load balancing, reactive power compensation, power factor correction, harmonics filtering and mitigation of other power quality issues. However, when solar irradiation is zero, in the night time, VSC acts as a DSTATCOM, which enhances the utilization factor of the system. Test results have been shown satisfactory performance of its operation at unity power factor under abnormal distribution network conditions, such as distortion in grid voltage at nonlinear and unbalance loading at PCC. Moreover, the THDs in grid voltage and grid current have been observed within the IEEE-519 standard.

References

[1] S. Yu, L. Zhang, H. H. C. Iu, T. Fernando and K. P. Wong, "A DSE-Based Power System Frequency Restoration Strategy for PV-Integrated Power Systems Considering Solar Irradiance Variations," *IEEE Trans. Industrial Informatics*, vol. 13, no. 5, pp. 2511-2518, Oct. 2017.

[2] N. Mahmud, A. Zahedi and A. Mahmud, "A Cooperative Operation of Novel PV Inverter Control Scheme and Storage Energy Management System Based on ANFIS for Voltage Regulation of Grid-Tied PV System," *IEEE Trans. Industrial Informatics*, vol. 13, no. 5, pp. 2657-2668, Oct. 2017.

[3] F. J. Lin, K. C. Lu and B. H. Yang, "Recurrent Fuzzy Cerebellar Model Articulation Neural Network Based Power Control of a Single-Stage Three-Phase Grid-Connected Photovoltaic System During Grid Faults," *IEEE Trans. Industrial Electronics*, vol. 64, no. 2, pp. 1258-1268, Feb. 2017.

[4] F. J. Lin, K. C. Lu, T. H. Ke, B. H. Yang and Y. R. Chang, "Reactive Power Control of Three-Phase Grid-Connected PV System During Grid Faults Using Takagi–Sugeno–Kang Probabilistic Fuzzy Neural Network Control," *IEEE Trans. Industrial Electronics*, vol. 62, no. 9, pp. 5516-5528, Sept. 2015.

[5] M. Cirrincione, M. Pucci, G. Vitale and A. Miraoui, "Current Harmonic Compensation by a Single-Phase Shunt Active Power Filter Controlled by Adaptive Neural Filtering," *IEEE Trans. Ind. Elect.*, vol. 56, no. 8, pp. 3128-3143, Aug. 2009.

[6] R. K. Agarwal, I. Hussain and B. Singh, "Implementation of LLMF Control Algorithm for Three-Phase Grid-Tied SPV-DSTATCOM System," *IEEE Trans. Industrial Electronics*, vol. 64, no. 9, pp. 7414-7424, Sept. 2017.

[7] S. Somkun and V. Chunkag, "Unified Unbalanced Synchronous Reference Frame Current Control for Single-Phase Grid-Connected Voltage-Source Converters," *IEEE Trans. Industrial Electronics*, vol. 63, no. 9, pp. 5425-5436, Sept. 2016.

[8] E. Kayacan, E. Kayacan, H. Ramon and W. Saeys, "Adaptive Neuro-Fuzzy Control of a Spherical Rolling Robot Using Sliding-Mode-Control-Theory-Based Online Learning Algorithm," *IEEE Trans. Cybernetics*, vol. 43, no. 1, pp. 170-179, Feb. 2013.

[9] A. Sangwongwanich, Y. Yang, F. Blaabjerg and D. Sera, "Delta Power Control Strategy for Multistring Grid-Connected PV Inverters," *IEEE Trans. Industry Applications*, vol. 53, no. 4, pp. 3862-3870, July-Aug. 2017.

[10] L. Tong , X. Zou, S. Shuai Feng, Y. Chen, Y. Kang, Q. Huang, and Y. Huang, "An SRF-PLL-Based Sensorless Vector Control Using the Predictive Deadbeat Algorithm for the Direct-Driven Permanent Magnet Synchronous Generator," *IEEE Trans. Power Electronics*, vol. 29, no. 6, pp. 2837-2849, June 2014.

[11] R. S. R. Chilipi, N. Al Sayari, K. H. Al Hosani and A. R. Beig, "Adaptive Notch Filter-Based Multipurpose Control Scheme for Grid-Interfaced Three-Phase Four-Wire DG Inverter," *IEEE Trans. Industry Applications*, vol. 53, no. 4, pp. 4015-4027, July-Aug. 2017.

[12] S. K. Chaudhary, R. Teodorescu, P. Rodriguez, P. C. Kjaer and A. M. Gole, "Negative Sequence Current Control in Wind Power Plants With VSC-HVDC Connection," *IEEE Trans. Sus. Energy*, vol. 3, no. 3, pp. 535-544, July 2012.

[13] P. Shah, I. Hussain and B. Singh, "Fuzzy Logic Based FOGI-FLL Algorithm for Optimal Operation of Single-Stage Three-Phase Grid Interfaced Multifunctional SECS," *IEEE Trans. Industrial Informatics*, vol. 14, no. 8, pp. 3334-3346, Aug. 2018.

[14] P. Shah, I. Hussain and B. Singh, "A Novel Fourth-Order Generalized Integrator Based Control Scheme for Multifunctional SECS in the Distribution System," *IEEE Trans. Energy Conversion*, vol. 33, no. 3, pp. 949-958, Sept. 2018.

[15] K. Shi and X. Ma, "A Frequency Domain Step-Size Control Method for LMS Algorithms," *IEEE Signal Processing Letters*, vol. 17, no. 2, pp. 125-128, Feb. 2010.

[16] A. Zerguine, C. F. N. Cowan and M. Bettayeb, "LMS-LMF adaptive scheme for echo cancellation," *Electronics Letters*, vol. 32, no. 19, pp. 1776-1778, 12 Sept. 1996.

[17] H. Zhu and H. Fujimoto, "Suppression of Current Quantization Effects for Precise Current Control of SPMSM Using Dithering Techniques and Kalman Filter," *IEEE Trans. Industrial Informatics*, vol. 10, no. 2, pp. 1361-1371, May 2014.

[18] N. Kumar, I. Hussain, B. Singh and B. K. Panigrahi, "Normal Harmonic Search Algorithm-Based MPPT for Solar PV System and Integrated With Grid Using Reduced Sensor Approach and PNKLMS Algorithm," *IEEE Trans. Industry Applic.*, vol. 54, no. 6, pp. 6343-6352, Nov.-Dec. 2018.

[19] Z. Wang, Y. Zheng, Z. Zou and M. Cheng, "Position Sensorless Control of Interleaved CSI Fed PMSM Drive With Extended Kalman Filter," *IEEE Trans. Magnetics*, vol. 48, no. 11, pp. 3688-3691, Nov. 2012.

[20] S. Golestan, J. M. Guerrero and J. C. Vasquez, "Steady-State Linear Kalman Filter-Based PLLs for Power Applications: A Second Look," *IEEE Trans. Industrial Electr.*, vol. 65, no. 12, pp. 9795-9800, Dec. 2018.

[21] M. B. Shadmand, R. S. Balog and H. Abu-Rub, "Model Predictive Control of PV Sources in a Smart DC Distribution System: Maximum Power Point Tracking and Droop Control," *IEEE Trans. Energy Conversion*, vol. 29, no. 4, pp. 913-921, Dec. 2014.

[22] A. Vidal, F. D. Freijedo, A. G. Yepes, J. Malvar, Ó. López and J. Doval-Gandoy, "Transient response evaluation of stationary-frame resonant current controllers for grid-connected applications," *IET Power Elect.*, vol. 7, no. 7, pp. 14-24, July 2014.

[23] S. B. Kjær, "Evaluation of the "Hill Climbing" and the "Incremental Conductance" Maximum Power Point Trackers for Photovoltaic Power Systems," *IEEE Trans. Energy Conversion*, vol. 27, no. 4, pp. 922-929, Dec. 2012.

[24] M. Killi and S. Samanta, "Modified Perturb and Observe MPPT Algorithm for Drift Avoidance in Photovoltaic Systems," *IEEE Trans. Industrial Electronics*, vol. 62, no. 9, pp. 5549-5559, Sept. 2015.

[25] N. Kumar, I. Hussain, B. Singh and B. K. Panigrahi, "Self-Adaptive Incremental Conductance Algorithm for Swift and Ripple-Free Maximum Power Harvesting From PV Array," *IEEE Trans. Industrial Informatics*, vol. 14, no. 5, pp. 2031-2041, May 2018.

[26] A. Al Nabulsi and R. Dhaouadi, "Efficiency Optimization of a DSP-Based Standalone PV System Using Fuzzy Logic and Dual-MPPT Control," *IEEE Trans. Industrial Informatics*, vol. 8, no. 3, pp. 573-584, Aug. 2012.

[27] D. D. Sabin and M. H. J. Bollen, "Overview of IEEE Std 1564-2014 Guide for Voltage Sag Indices," *2014 16th International Conference Harmonics and Quality of Power (ICHQP)*, Bucharest, 2014, pp. 497-501.

[28] M Gönen, E. Alpaydm, "Multiple kernel learning algorithms", The Journal of Machine Learning Research, vol. 12, pp. 2211-2268, 2011.

[29] N. Kumar, B. Singh, B. Ketan Panigrahi, C. Chakraborty, H. M. Suryawanshi and V. Verma, "Integration of Solar PV with Low-Voltage Weak Grid System: Using Normalized Laplacian Kernel Adaptive Kalman Filter and Learning Based InC Algorithm," *IEEE Transactions on Power Electronics*.

[30] N. Kumar, B. Singh and B. K. Panigrahi, "Integration of Solar PV with Low-Voltage Weak Grid System: using Maximize-M Kalman Filter and Self-tuned P&O Algorithm," *IEEE Transactions on Industrial Electronics*.

[31] N. Kumar, B. Singh and B. K. Panigrahi, "Framework of Gradient Descent Least Squares Regression Based NN Structure for Power Quality Improvement in PV Integrated Low-Voltage Weak Grid System," *IEEE Transactions on Industrial Electronics*.

[32] N. Kumar, B. Singh and B. K. Panigrahi, "LLMLF based Control Approach and LPO MPPT Technique for Improving Performance of a Multifunctional Three-Phase Two-Stage Grid Integrated PV System," *IEEE Transactions on Sustainable Energy*.

[33] N. Kumar, B. Singh, B. K. Panigrahi and L. Xu, "Leaky Least Logarithmic Absolute Difference Based Control Algorithm and Learning Based InC MPPT Technique for Grid Integrated PV System," *IEEE Transactions on Industrial Electronics*.

[34] N. Kumar, B. Singh, and B. K. Panigrahi "Grid synchronisation framework for partially shaded solar PV-based microgrid using intelligent control strategy", IET Generation, Transmission & Distribution, 2018.

[35] N. Kumar, I. Hussain, B. Singh and B. K. Panigrahi, "Single sensor based MPPT for partially shaded solar photovoltaic by using human psychology optimisation algorithm," *IET Generation, Transmission & Distribution*, vol. 11, no. 10, pp. 2562-2574, 13 7 2017.

[36] N. Kumar, S. Majumdar and G. M. Babu, "Automatic control of tidal power plant," *2012 International Conference on Emerging Trends in Electrical Engineering and Energy Management (ICETEEEM)*, Chennai, 2012, pp. 24-28.

[37] N. Kumar, T. Mulo and V. P. Verma, "Application of computer and modern automation system for protection and optimum use of High voltage power transformer," *2013 International Conference on Computer Communication and Informatics*, Coimbatore, 2013, pp. 1-5.

[38] S. K. Saha, R. Kar, T. I. Mandai, N. Kumar and S. P. Ghoshal, "Optimal linear phase fir high pass filter design using PSOCFIWA-WM," *2012 World Congress on Information and Communication Technologies*, Trivandrum, 2012, pp. 768-773.

Nishant Kumar (M'15), received the M.Tech. (Gold Medalist) degree in electrical power system from the National Institute of Technology Durgapur, Durgapur, WB, India, in 2013. He is currently working toward the Ph.D. degree in power system in the Department of Electrical Engineering, Indian Institute of Technology (IIT) Delhi, New Delhi, India.

From 2013 to 2014, he was the Project Engineer/Research Associate with IIT Bombay and IIT Delhi. His areas of research interests include soft computing based generation control, optimization algorithm development, and application of soft computing techniques in power system planning, operation and control.

He has received Gold Medal in M.Tech degree from National Institute of Technology Durgapur, India in the year 2013, and POSOCO Power System National Award (PPSA-2018) in Doctoral Category, from Power Grid Corporation of India Limited, in the year 2018.

Bhim Singh (SM'99, F'10) was born in Rahamapur, Bijnor, UP, India, in 1956. He received the B.E. degree in electrical from the University of Roorkee, Roorkee, India, in 1977, and the M.Tech. degree in power apparatus and systems and the Ph.D. degree in electrical machine from Indian Institute of Technology (IIT) Delhi, New Delhi, India, in 1979 and 1983, respectively.

In 1983, he joined the Department of Electrical Engineering, University of Roorkee (now IIT Roorkee), as a Lecturer. He became a Reader there in 1988. In December 1990, he joined the Department of Electrical Engineering, IIT Delhi, as an Assistant Professor, where he has become an Associate Professor in 1994 and a Professor in 1997. He has been the Head in the Department of Electrical Engineering, IIT Delhi, from July 2014 to August 2016. He is currently the Dean, Academics with IIT Delhi. He has guided 74 Ph.D. dissertations, 166 M.E./M.Tech./M.S.(R) thesis. He has executed more than 75 sponsored and consultancy projects.

His areas of research interests include PV grid interface systems, microgrid, power quality, PV water pumping systems, power electronics, electrical machines, drives, FACTS, and HVdc systems.

Bijaya Ketan Panigrahi (SM'06) received the Ph.D. degree in power system from Sambalpur University, Sambalpur, India, in 2004.

He was a Lecturer with the University College of Engineering, Sambalpur, for 13 years. Since 2005, he has been an Associate Professor in the Department of Electrical Engineering, Indian Institute of Technology (IIT) Delhi, New Delhi, India, where he has become a Professor in 2017.

His research interests include intelligent control of flexible ac transmission system devices, digital signal processing, power quality assessment, and application of soft computing techniques to power system planning, operation and control.